Neurosci. Bull. September, 2023, 39(9):1459–1462
https://doi.org/10.1007/s12264-023-01071-4

www.neurosci.cn
www.springer.com/12264

LETTER TO THE EDITOR

Lypd1-DTR/+: A New Mouse Model for Specifically Damaging the Type Ic Spiral Ganglion Neurons of the Cochlea

Di Zhang[1,2] · Minhui Ren[1,2] · ZhengHong Bi[1] · Yunpeng Gu[1,2] · Shuting Li[1,2] · Guangqin Wang[1,2] · Xiang Li[1] · Zhiyong Liu[1,2,3]

Received: 16 February 2023 / Accepted: 7 May 2023 / Published online: 24 May 2023

Dear Editor,

Inner ear auditory neurons, which are also referred as to spiral ganglion neurons (SGNs), bridge sound-receptor hair cells (HCs) to the cochlear nucleus in the brainstem [1]. Two types of SGN exist: type I SGNs (95%), which innervate inner HCs (IHCs), and type II SGNs (only 5%), which form synapses with outer HCs (OHCs) [1, 2]. Recent transcriptomic studies have revealed the heterogeneity within type I SGNs, which can be further divided into three distinct subtypes: Ia, Ib, and Ic [3–5]; these three subtypes first emerge at E16 and are refined over the first postnatal week [6, 7]. Although no molecular markers have thus far been found to show complete "ON" or "OFF" expression patterns in the subtypes, several genes display marked expression gradients among Ia, Ib, and Ic [3–5]. Ly6/Plaur domain containing 1, which is encoded by *Lypd1* (also known as *Lynx2*), belongs to the Ly-6/neurotoxin superfamily and is involved in modulating the activity of nicotinic acetylcholine receptors [8]. Notably, *Lypd1* is expressed at the highest level in type Ic SGNs and minimally expressed in Ib and Ia SGNs in adult cochleae [3–5]. Moreover, two intrinsic transcription factors, Neurod1 and Runx1, promote the entry of undifferentiated SGN precursors into the Ic or Ic/Ib differentiation track [6, 9]. Lastly, IHC-driven activity through synapses between IHCs and SGNs is also required in the diversification of type I SGNs [3, 4]. Vesicular glutamate transporter type 3 (vGlut3, encoded by *Slc17a8*) is essential for glutamate release from IHCs [10, 11], and, accordingly, *vGlut3*$^{-/-}$ mice show drastically reduced percentages of type Ic SGNs and overproduction of type Ia SGNs expressing high levels of Calb2 [3, 4].

Type Ic SGNs present a few notable features: First, they have a low spontaneous firing rate [3]; second, they form synapses with larger presynaptic ribbons at the modiolar side of IHCs [3–5]; and third, they are selectively vulnerable to aging [3]. Thus, degeneration of type Ic SGNs in mice is expected to closely mimic human age-related hearing loss (ARHL), or presbycusis, the most common form of sensory impairment among older adults [12]. However, a mouse model with specific damage of type Ic SGNs is not yet available.

Here, we generated a new mouse model: *Lypd1**3×V5-P2A-DTR/+ (*Lypd1*-DTR/+, in short); we applied the diphtheria toxin (DT)/DT receptor (DTR) system, which is widely used to achieve cell-type-specific damage in the inner ear [13]. By using CRISPR/Cas9-mediated homologous recombination in mouse zygotes [14], we inserted a DNA fragment containing 3×V5-P2A-DTR immediately before the stop codon (TGA) of *Lypd1* (Fig. S1A–C). Thus, DTR would be expressed, in principle, under the control of endogenous *Lypd1* promoters and enhancers. Moreover, because three V5 tags are fused to the C-terminus of Lypd1

Di Zhang and Minhui Ren have contributed equally to this work.

Supplementary Information The online version contains supplementary material available at https://doi.org/10.1007/s12264-023-01071-4.

✉ Xiang Li
lixiang@ion.ac.cn

✉ Zhiyong Liu
Zhiyongliu@ion.ac.cn

[1] Institute of Neuroscience, State Key Laboratory of Neuroscience, CAS Center for Excellence in Brain Science and Intelligence Technology, Chinese Academy of Sciences, Shanghai 200031, China

[2] University of Chinese Academy of Sciences, Beijing 100049, China

[3] Shanghai Center for Brain Science and Brain-Inspired Intelligence Technology, Shanghai 201210, China

here, a V5 antibody can be used to visualize Lypd1 protein expression. Tail-DNA PCR analysis readily distinguished wild-type (WT), heterozygous, and homozygous knockin (KI) littermates (Fig. S1D). Southern blotting using a DTR probe (blue line in Fig. S1C) further revealed that, besides being correctly targeted into the *Lypd1* locus as designed, the targeting vector was randomly inserted in one unknown location in the mouse genome. Because random insertion frequently occurs in inactive regions of the genome, we suspected that *Lypd1*-DTR/+ could still be used to specifically damage Lypd1$^+$ type Ic SGNs. Alternatively, *Lypd1*-DTR/+ could at least serve as a pseudo-transgenic mouse line, as confirmed by our assays below.

We first assessed the degree to which V5 expression recapitulated the previously reported expression pattern of endogenous Lypd1 [3–5]. Triple staining of V5, the pan-SGN marker Map2, and the glial-cell marker Sox2 revealed that V5$^+$/Map2$^+$ SGNs accounted for 26.8 ± 1.8% (n = 3) of the total Map2$^+$ SGNs in *Lypd1*-DTR/+ mice at P28, which matched the 24–25% reported in the adult WT cochlea. To further show that V5 expression can faithfully reflect Lypd1 expression, we compared the proportion of V5$^+$/Map2$^+$ SGNs between *Lypd1*-DTR/+ (Fig. 1A–A’’’) and *Lypd1*-DTR/+; *vGlut3*$^{-/-}$ mice at P28 (Fig. 1B–B’’’). As expected, the percentage of V5$^+$/Map2$^+$ SGNs dropped significantly (P <0.001), from 26.8 ± 1.8% (n = 3) in *Lypd1*-DTR/+ to 6.6 ± 1.5% (n = 3) in *Lypd1*-DTR/+; *vGlut3*$^{-/-}$ (Fig. 1C). Conversely, triple staining of Map2, Calb2 (a marker enriched in type Ia SGNs), and Sox2 showed that the percentage of Calb2$^+$/Map2$^+$ SGNs increased from 65.4 ± 4.9% (n = 3) in *Lypd1*-DTR/+ to 86.1 ± 2.4% (n = 3) in *Lypd1*-DTR/+; *vGlut3*$^{-/-}$ at P28 (Fig.1D–F). Notably, V5 (Lypd1) was not detected in any Sox2$^+$ glial cell. Thus, our results agreed with the previous finding that the percentage of type Ic SGNs is drastically lower in *vGlut3*$^{-/-}$ mice than in control mice [3, 4].

Dual labeling for V5 and Calb2 further revealed a minimal overlap of their expression in SGNs at P28 (Fig. S2); Calb2 is enriched in type Ia and Ib SGNs but is minimally expressed in type Ic SGNs [3–5]. Most V5+ SGNs did not

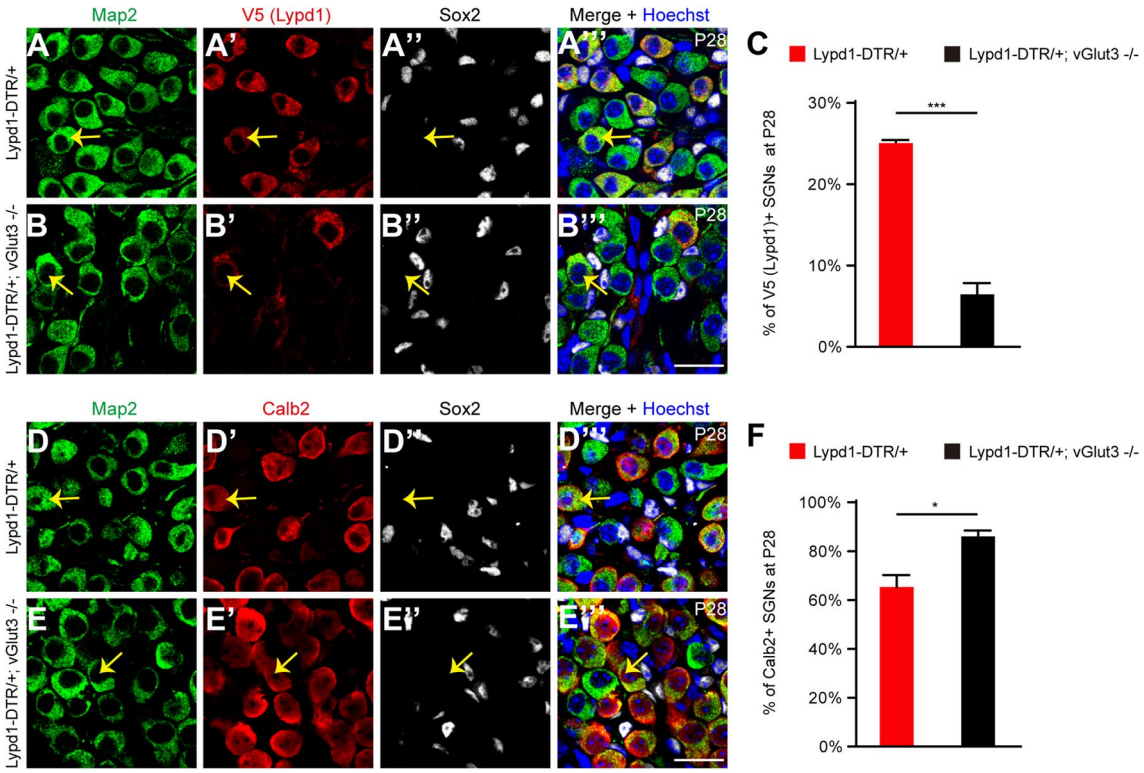

Fig. 1 Visualization of type Ic SGNs by using V5 expression in the *Lypd1*-DTR/+ model. **A–B’’’** Triple staining of Map2, V5, and Sox2 in *Lypd1*-DTR/+ (**A–A’’’**) and *Lypd1*-DTR/+; *vGlut3*$^{-/-}$ (**B–B’’’**) mice. All V5$^+$ cells express the pan-SGN marker Map2. Yellow arrows: V5$^+$/Map2$^+$ SGNs. V5 expression was not detected in any Sox2$^+$ glial cells. **C** Percentages of V5$^+$/Map2$^+$ SGNs (type Ic) among all SGNs: *Lypd1*-DTR/+ (red) *vs* *Lypd1*-DTR/+; *vGlut3*$^{-/-}$ (black) mice at P28. ***P <0.001. **D–E’’’** Triple staining of Map2, Calb2, and Sox2 in *Lypd1*-DTR/+ (**D–D’’’**) and *Lypd1*-DTR/+; *vGlut3*$^{-/-}$ (**E–E’’’**) mice at P28. Calb2 (Calretinin) is expressed in a fraction of Map2$^+$ SGNs, but not in any Sox2$^+$ glial cells. Yellow arrows: Calb2$^+$/Map2$^+$ SGNs. **F** Percentages of Calb2$^+$/Map2$^+$ SGNs among all SGNs: *Lypd1*-DTR/+ (red) *vs* *Lypd1*-DTR/+; *vGlut3*$^{-/-}$ (black) mice at P28. n = 3 for each model, *P <0.05. Scale bars, 20 μm.

express Calb2 (white arrows in Fig. S2A–A''), and only 5.3 ± 2.5% of the V5$^+$ SGNs were Calb2$^+$ (yellow arrows in Fig. S2B–B''); moreover, Calb2 expression in these V5$^+$ SGNs was lower than that in other nearby Calb2$^+$ SGNs that did not express Lypd1 (V5) (Fig. S2B–B''). Similarly, among the Calb2$^+$ SGNs, only 1.8 ± 0.9% of the cells were V5$^+$. Collectively, these results showed that despite the random vector insertion in the *Lypd1*-DTR/+ mouse genome, the V5 expression pattern resembled the previously reported *Lypd1* mRNA expression pattern in adult SGNs [3–5]. Thus, we reason that DTR is primarily expressed in type Ic SGNs and that *Lypd1*-DTR/+ is a suitable model for ablating Lypd1$^+$ Ic SGNs through DT administration at adult ages.

Next, we characterized the SGN cell-death pattern in *Lypd1*-DTR/+ mice treated with or without a single dose of DT (25 ng/g body weight) at P31 and then analyzed at P38. Compared with *Lypd1*-DTR/+ mice not treated with DT (control, "no DT") (Fig. 2A–A'''), DT-treated *Lypd1*-DTR/+ mice showed the loss of a majority of V5$^+$ SGNs (Fig. 2B–B'''); in the control mice, the percentage of V5$^+$ (Lypd1$^+$) type Ic SGNs was 25.2 ± 0.3% (n = 3), but this dropped markedly, to 0.8 ± 0.3% (n = 3), in DT-treated mice (Fig. 2C). In accordance with this specific loss of Ic SGNs, the total number of Map2$^+$/Sox2$^-$ SGNs in the DT-treated mice (290.8 ± 7.4, n = 3) was also significantly lower than that (341.2 ± 4.4, n = 3) in no-DT-treated mice (Fig. 2D).

Lastly, we quantified the hearing ability of *Lypd1*-DTR/+ mice by measuring the auditory brainstem response (ABR): the hearing thresholds at all frequencies in DT-treated mice (red line in Fig. 2E) were significantly higher than their counterparts in no DT-treated *Lypd1*-DTR/+ mice (green line in Fig. 2E). Thus, the hearing ability was substantially impaired in DT-treated mice. Furthermore, analysis of WT mice treated with an identical single dose of DT revealed no significant difference in ABR threshold/hearing function between the DT-treated WT (blue line in Fig. 2E) and no DT-treated *Lypd1*-DTR/+ mice (green line in Fig. 2E), eliminating the possibility that DT treatment itself affects the hearing of mice.

Two lines of evidence support the view that *Lypd1*-DTR/+ is a reliable model for visualizing type Ic SGNs. First, we found here that the percentage of V5$^+$/Map2$^+$

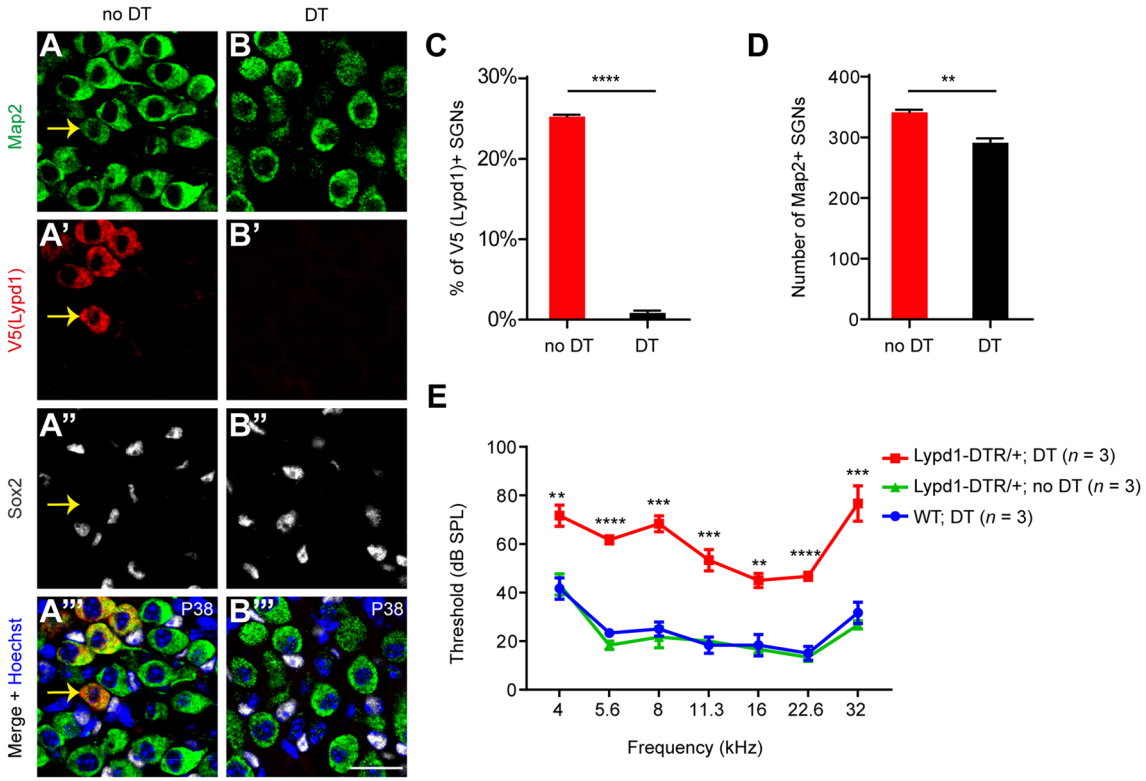

Fig. 2 The V5$^+$ (Lypd1$^+$) SGNs are specifically damaged in adult *Lypd1*-DTR/+ mice after DT treatment. **A–B'''** Triple staining of Map2, V5, and Sox2 in *Lypd1*-DTR/+ mice without (**A–A'''**) and with single-dose DT treatment at P31 (**B–B'''**). All samples were analyzed at P38. Arrows in (**A–A'''**): one V5$^+$/Map2$^+$ type Ic SGN. Almost all V5$^+$ SGNs disappeared in DT-treated mice (**B–B'''**). **C** Percentages of V5$^+$ SGNs in no-DT-treated (red) and DT-treated (black) *Lypd1*-DTR/+ mice at P38. ****P <0.0001. **D** Total numbers of Map2$^+$ SGNs in no-DT-treated (red) and DT-treated (black) *Lypd1*-DTR/+ mice at P38. **P <0.01. **E** ABR measurements from wild-type mice with DT treatment (blue line) and *Lypd1*-DTR/+ mice without (green line) or with DT treatment (red line). n = 3 for each model, **P <0.01, ***P <0.001, ****P <0.0001. Scale bar, 20 µm.

SGNs was 25.2–26.8%, which is close to the ~24% reported in three previous studies [3–5]. Second, when V5 expression was used as the readout, the percentage of type Ic SGNs was measured to be drastically decreased in *vGlut3*$^{-/-}$ mutants as reported before [3, 4]. Thus, the V5 expression faithfully recapitulated the expression pattern of endogenous Lypd1. More importantly, the near absence of V5^{+} SGNs in *Lypd1*-DTR/+ mice after treatment with a single dose of DT confirmed that type Ic SGNs were selectively ablated, implicating *Lypd1*-DTR/+ as a useful model in which to mimic human ARHL.

Considerable research effort has been devoted to converting cochlear glial cells into SGNs [15–17] because this represents a promising approach for regenerating SGNs *in situ*. We previously showed that Neurod1 and Neurog1 expression can convert glial cells into nascent SGNs, but adult glial cells are not responsive to ectopic Neurod1 and Neurog1 expression [16]. Whether pre-damaging endogenous SGNs would increase the reprogramming efficiency of Neurod1 and Neurog1 remains unknown. Ouabain has been used to damage type I SGNs [18], but ouabain does not show selectivity for the type I SGN subtype. To the best of our knowledge, *Lypd1*-DTR/+ is the first genetic model that allows selective damage of type Ic SGNs. It will be of interest to determine whether glial cells tend to transdifferentiate into type Ic SGNs only if endogenous type Ic SGNs are specifically damaged. In summary, we have successfully established the *Lypd1*-DTR/+ mouse model that could be used to visualize and ablate type Ic SGNs.

Acknowledgements We thank Dr. Qian Hu from the Optical Imaging Facility of the ION for support with image analysis, and Ms. Qian Liu from the Department of Embryology of the ION animal center for helping us in transplanting zygotes into pseudopregnant female mice. This work was supported by the National Key R&D Program of China (2021YFA1101804), the National Natural Science Foundation of China (82000985 and 82101217), the Strategic Priority Research Program of Chinese Academy of Science (XDB32060100), and a Shanghai Municipal Science and Technology Major Project (2018SHZDZX05).

References

1. Li C, Li X, Bi Z, Sugino K, Wang G, Zhu T. Comprehensive transcriptome analysis of cochlear spiral ganglion neurons at multiple ages. Elife 2020, 9: e50491.
2. Li J, Liu S, Song C, Zhu T, Zhao Z, Sun W, *et al*. Prestin-mediated frequency selectivity does not cover ultrahigh frequencies in mice. Neurosci Bull 2022, 38: 769–784.
3. Shrestha BR, Chia C, Wu L, Kujawa SG, Liberman MC, Goodrich LV. Sensory neuron diversity in the inner ear is shaped by activity. Cell 2018, 174: 1229-1246.e17.
4. Sun S, Babola T, Pregernig G, So KS, Nguyen M, Su SM, *et al*. Hair cell mechanotransduction regulates spontaneous activity and spiral ganglion subtype specification in the auditory system. Cell 2018, 174: 1247-1263.e15.
5. Petitpré C, Wu H, Sharma A, Tokarska A, Fontanet P, Wang Y, *et al*. Neuronal heterogeneity and stereotyped connectivity in the auditory afferent system. Nat Commun 2018, 9: 3691.
6. Petitpré C, Faure L, Uhl P, Fontanet P, Filova I, Pavlinkova G, *et al*. Single-cell RNA-sequencing analysis of the developing mouse inner ear identifies molecular logic of auditory neuron diversification. Nat Commun 2022, 13: 3878.
7. Sanders TR, Kelley MW. Specification of neuronal subtypes in the spiral ganglion begins prior to birth in the mouse. Proc Natl Acad Sci U S A 2022, 119: e2203935119.
8. Tekinay AB, Nong Y, Miwa JM, Lieberam I, Ibanez-Tallon I, Greengard P, *et al*. A role for LYNX2 in anxiety-related behavior. Proc Natl Acad Sci U S A 2009, 106: 4477–4482.
9. Shrestha BR, Wu L, Goodrich LV. Runx1 controls auditory sensory neuron diversity in mice. Dev Cell 2023, 58: 306-319.e5.
10. Ruel J, Emery S, Nouvian R, Bersot T, Amilhon B, Van Rybroek JM, *et al*. Impairment of SLC17A8 encoding vesicular glutamate transporter-3, VGLUT3, underlies nonsyndromic deafness DFNA25 and inner hair cell dysfunction in null mice. Am J Hum Genet 2008, 83: 278–292.
11. Seal RP, Akil O, Yi E, Weber CM, Grant L, Yoo J, *et al*. Sensorineural deafness and seizures in mice lacking vesicular glutamate transporter 3. Neuron 2008, 57: 263–275.
12. Bowl MR, Dawson SJ. Age-related hearing loss. Cold Spring Harb Perspect Med 2019, 9: a033217.
13. Sun S, Li S, Luo Z, Ren M, He S, Wang G, *et al*. Dual expression of Atoh1 and Ikzf2 promotes transformation of adult cochlear supporting cells into outer hair cells. Elife 2021, 10: e66547.
14. Li C, Shu Y, Wang G, Zhang H, Lu Y, Li X, *et al*. Characterizing a novel vGlut3-P2A-iCreER knockin mouse strain in cochlea. Hear Res 2018, 364: 12–24.
15. Wakizono T, Nakashima H, Yasui T, Noda T, Aoyagi K, Okada K, *et al*. Growth factors with valproic acid restore injury-impaired hearing by promoting neuronal regeneration. JCI Insight 2021, 6: e139171.
16. Li X, Bi Z, Sun Y, Li C, Li Y, Liu Z. *In vivo* ectopic Ngn1 and Neurod1 convert neonatal cochlear glial cells into spiral ganglion neurons. FASEB J 2020, 34: 4764–4782.
17. Noda T, Meas SJ, Nogami J, Amemiya Y, Uchi R, Ohkawa Y, *et al*. Direct reprogramming of spiral ganglion non-neuronal cells into neurons: Toward ameliorating sensorineural hearing loss by gene therapy. Front Cell Dev Biol 2018, 6: 16.
18. Lang H, Schulte BA, Schmiedt RA. Ouabain induces apoptotic cell death in type I spiral ganglion neurons, but not type II neurons. J Assoc Res Otolaryngol 2005, 6: 63–74.